PNAS RESEARCH ARTICLE | CELL BIOLOGY

# Ubiquitin-induced RNF168 condensation promotes DNA double-strand break repair

Li-Li Feng[a,b,c,d,1], Shu-Ying Bie[e,1], Zhi-Heng Deng[f,1], Shao-Mei Bai[e,1], Jie Shi[e,g,h], Cao-Litao Qin[e,g,h], Huan-Lei Liu[a,b,i,j], Jia-Xu Li[a,b,i,j], Wan-Ying Chen[j], Jin-Ying Zhou[a,b,i,j], Chun-Mei Jiao[a,b,i,j], Yi Ma[e], Meng-Bo Qiu[j], Hua-Song Ai[f], Jian Zheng[e,g,h], Mien-Chie Hung[k,2], Yun-Long Wang[a,b,i,j,2], Xiang-Bo Wan[a,b,i,j,2], and Xin-Juan Fan[a,b,j,2]

Affiliations are included on p. 11.

Edited by Ronald DePinho, MD Anderson Cancer Center, The University of Texas, Houston, TX; received January 1, 2024; accepted May 22, 2024

**Rapid accumulation of repair factors at DNA double-strand breaks (DSBs) is essential for DSB repair. Several factors involved in DSB repair have been found undergoing liquid–liquid phase separation (LLPS) at DSB sites to facilitate DNA repair. RNF168, a RING-type E3 ubiquitin ligase, catalyzes H2A.X ubiquitination for recruiting DNA repair factors. Yet, whether RNF168 undergoes LLPS at DSB sites remains unclear. Here, we identified K63-linked polyubiquitin-triggered RNF168 condensation which further promoted RNF168-mediated DSB repair. RNF168 formed liquid-like condensates upon irradiation in the nucleus while purified RNF168 protein also condensed in vitro. An intrinsically disordered region containing amino acids 460–550 was identified as the essential domain for RNF168 condensation. Interestingly, LLPS of RNF168 was significantly enhanced by K63-linked polyubiquitin chains, and LLPS largely enhanced the RNF168-mediated H2A.X ubiquitination, suggesting a positive feedback loop to facilitate RNF168 rapid accumulation and its catalytic activity. Functionally, LLPS deficiency of RNF168 resulted in delayed recruitment of 53BP1 and BRCA1 and subsequent impairment in DSB repair. Taken together, our finding demonstrates the pivotal effect of LLPS in RNF168-mediated DSB repair.**

DNA double-strand break repair | intrinsically disordered region | liquid–liquid phase separation | polyubiquitin | RNF168

## Significance

We demonstrated that RNF168 underwent liquid–liquid phase separation at the double-strand break (DSB) sites driven by both the intrinsically disordered region and the interaction with K63-linked polyubiquitin chains. Irradiation-induced RNF168 condensation accelerated the accumulation of RNF168 and promoted the recruitment of downstream factors to DSB, resulting in enhanced DSB repair. Our finding is expected to provide a potential target for the prevention and intervention of irradiation damage.

DNA double-strand break (DSB) is the common and most toxic DNA lesion that leads to genomic instability and oncogenic mutations (1, 2). Therefore, DSBs are tightly monitored, and the repair of DSBs is strictly regulated. Upon initial sensing of DSBs by the MRE11/RAD50/NBS1 (MRN) complex, H2A.X is phosphorylated at Ser139 (γ-H2A.X) by activated ataxia telangiectasia-mutated (ATM) kinase (3–5), providing a scaffold for recruiting MDC1 and RNF8 (6). Subsequently, RNF168 binds to the ubiquitinated H1 catalyzed by RNF8 and mediates K63-linked ubiquitination of H2A.X (7, 8), which further functions as a scaffold for recruiting downstream factors such as 53BP1 and BRCA1 (9, 10). Finally, DSBs are repaired through a nonhomologous end joining (NHEJ) or homologous recombination (HR) pathway (11, 12).

Many posttranslational modifications are employed on histones to enhance the chromatin accessibility to DNA repair factors (13). The mutation of RNF168, a RING finger protein endowed with E3 ubiquitin ligase activity, was first identified as the underlying genetic cause for RIDDLE (radiosensitivity, immunodeficiency, dysmorphic features, and learning difficulties) syndrome in 2009 (14). Patients with RIDDLE syndrome are deficient in DSB repair and highly sensitive to irradiation-induced cell death (15, 16). RNF168 is initially recruited to DSB sites by interacting with the RNF8-catalyzed ubiquitin chain on H1.2 by its ubiquitin-interacting motifs (6, 17). Subsequently, RNF168 triggers the H2A.X monoubiquitination at K13/15 and amplifies the K63-linked poly-ubiquitination, which is considered as a rate-limiting step to recruit key DSBs repair factors, such as 53BP1 and BRCA1 (9, 10). The recruitment of these factors is ascribed to the direct association between factors and ubiquitinated conjugates and is identified as a dominant step for DSB repair initiation and repair pathway choice (18). Therefore, the rapid and highly concentrated accumulation of RNF168 and subsequent ubiquitination of H2A.X are essential for DSB repair. However, in addition to the physical interaction between RNF168 and ubiquitinated H1.2, if any other mechanisms, such as LLPS, are involved in the rapid accumulation of RNF168 needs to be futher investigated.

Until very recently, liquid–liquid phase separation (LLPS) is identified as the driving force of many macromolecules' condensation, such as membraneless organelles

Author contributions: M.-C.H., Y.-L.W., X.-B.W., and X.-J.F. designed research; L.-L.F., S.-Y.B., S.-M.B., H.-L.L., J.-X.L., W.-Y.C., J.-Y.Z., C.-M.J., Y.M., and M.-B.Q. performed research; Z.-H.D., J.S., C.-L.Q., H.-S.A., and J.Z. provided methodological assistance; L.-L.F. S.-Y.B., S.-M.B., and Y.-L.W. analyzed data; and L.-L.F., S.-Y.B., and Y.-L.W. wrote the paper.

The authors declare no competing interest.

This article is a PNAS Direct Submission.



[1]L.-L.F., S.-Y.B., Z.-H.D., and S.-M.B. contributed equally to this work.

[2]To whom correspondence may be addressed. Email: mhung@cmu.edu.tw, wangylong@zzu.edu.cn, wanxbo@zzu.edu.cn, or fanxjuan@zzu.edu.cn.

This article contains supporting information online at https://www.pnas.org/lookup/suppl/doi:10.1073/pnas.2322972121/-/DCSupplemental.

Published July 5, 2024.

(19, 20). Our and other studies have reported that LLPS plays key roles in the recruitment and accumulation of several DSB repair factors (21, 22). In 2015, Altmeyer et al. found that PARP1-induced poly (ADP-ribose) (PAR) at DSBs seeded a liquid core for highly disordered proteins' condensation and facilitated DNA repair (23, 24). As the first characterized DSB repair factor with LLPS property, 53BP1 undergoes LLPS via binding to DNA damage–induced long noncoding RNAs (dilncRNAs), which promotes DSB repair and DSB-induced p53 activation (25–27). Considering that various types of post-translational modifications are involved in the DSB process, whether there are different mechanisms driving LLPS of repair factor needs to be further disclosed.

In this study, we characterized that RNF168 formed liquid-like condensation at DSB sites in an intrinsically disordered region (IDR)-dependent manner. Interestingly, we found that K63-linked polyubiquitin chains, the irradiation-induced modification on chromatin catalyzed by RNF168, remarkably enhanced RNF168 LLPS in vitro. Most importantly, LLPS deficiency reduced RNF168 accumulation and it-mediated H2A.X ubiquitination at DSBs, which further decreased downstream factors recruitment and impaired the DNA damage repair. This study uncovers a mechanism for spatiotemporal regulation in DSB response.

## Results

**RNF168 Forms Liquid-Like Condensates at DNA Damage Sites.** We have previously identified several DNA repair factors with the property of LLPS and found that multivalent interactions with polyubiquitin induced LLPS at DSB sites (21, 22). Therefore, we probed into the possibility that RNF168, an E3 ligase that initially interacts with ubiquitinated H1 and subsequently induces ubiquitination of H2A.X, might undergo LLPS at DSB sites. Disordered region analysis using PONDR (http://www.pondr.com) showed that RNF168 harbored two dominant disordered regions (defined as IDR1 and IDR2, respectively), a characteristic of proteins undergoing LLPS (Fig. 1*A*). Consistently, RNF168-mEGFP protein spontaneously formed liquid-like condensates when highly expressed in HEK 293T cells, which was not obviously observed in low expression level (Fig. 1 *B* and *C*). The condensation of RNF168 was not impacted by the terminal location of mEGFP tag (*SI Appendix*, Fig. S1*A*) and could be dissolved by 1,6-hexanediol treatment (*SI Appendix*, Fig. S1*B*). Endogenous RNF168 dispersedly distributed in the nucleus but formed puncta at DSB sites after X-ray irradiation which could be observed in different cell lines (HeLa, NCM460, and RKO) (Fig. 1*D* and *SI Appendix*, Fig. S1*C*). Exogenous RNF168-mEGFP protein also accumulated at microirradiated regions (*SI Appendix*, Fig. S1*D*). Interestingly, the size of irradiation-induced RNF168 puncta increased along with time extension (Fig. 1*E*), while adjacent puncta could dynamically fuse into a larger condensate (*SI Appendix*, Fig. S1*E*). Fluorescence recovery after photobleaching (FRAP) assays were conducted to verify the mobility of RNF168 condensates. Both spontaneously formed and irradiation-induced RNF168 condensates rapidly recovered within 60 s after photobleaching (Fig. 1 *F* and *G* and *SI Appendix*, Fig. S1*F*). The fluorescence of a photobleached region within RNF168 condensates also recovered rapidly (Fig. 1*H*), supporting the liquid-like property of RNF168 condensates. Additionally, disrupting LLPS by 1,6-hexanediol before irradiation suppressed the foci formation of RNF168 (*SI Appendix*, Fig. S1*G*). Moreover, irradiation-induced RNF168 foci could also be dissolved by 1,6-hexanediol, indicating that RNF168 underwent LLPS at DSB sites (*SI Appendix*, Fig. S1*H*).

Consistently, the in vitro assay showed that purified RNF168 proteins dyed with fluorescence label TAMRA formed spherical condensates in the solution with crowding reagent polyethylene glycol 8000 (PEG8000, 5%) (Fig. 1*I* and *SI Appendix*, Fig. S1*I*). Condensation of RNF168 proteins was accelerated by higher protein concentration, lower salt content, and higher acidity (Fig. 1*J*). These results show that highly disordered protein RNF168 undergoes LLPS in vitro or in cells with high RNF168 expression level, while RNF168 puncta at DSB sites also have liquid-like properties.

**Disordered Region 460–550aa Is Essential for the LLPS of RNF168.** We next asked whether there was the dominant region responsible for the LLPS of RNF168. RNF168 mainly consists of a RING motif and two IDRs (IDR1 and IDR2) (Fig. 2*A*). Truncation assays indicated that deletion of IDR1 (ΔIDR1) significantly reduced the condensation, while deletion of IDR2 (ΔIDR2) completely abolished the LLPS of RNF168-mEGFP (Fig. 2*B*). Deficiency of RING (ΔRING) seemed to retain fewer but larger puncta with burr-like margin (Fig. 2*B*). Additionally, the in vitro assay showed that purified IDR2 instead of IDR1 formed condensates (Fig. 2*C* and *SI Appendix*, Fig. S2*A*). The IDR2-mEGFP condensates presented a smooth surface as shown in atomic force microscope (AFM) imaging (Fig. 2*D*). Condensation of IDR2 protein was closely correlated with protein concentration and salt content, which was similar to wild-type RNF168 protein (Fig. 2*E*). Furthermore, an optoIDR assay was used to further examine the LLPS property of IDR2 (28). The recombinant IDR2-Cry2-mCherry formed liquid-like puncta upon exposure to blue light (488 nm) (Fig. 2*F* and *SI Appendix*, Fig. S2*B*), which were sensitive to 1,6-hexanediol treatment (*SI Appendix*, Fig. S2*C*) and partly recovered after photobleaching (Fig. 2*G*). We therefore considered IDR2 as the dominant region for LLPS of RNF168.

The IDR2 (323–550aa) contains more than 220 amino acids and includes an MIU2 (motif interacting with Ub) domain (443–459aa), which is reported to bind ubiquitinated substrates and is essential for RNF168 recruitment. We further narrowed down the key IDR by separating IDR2 at MIU2 into an anterior region (323–442aa) and a posterior region (460–550aa). As shown, deletion of 460–550aa (Δ460–550aa) almost abolished the LLPS of RNF168 in cells, while deletion of 323–442aa (Δ323–442aa) retained apparent foci formation (Fig. 2*H*). Consistent with the cellular observation, purified IDR2-Δ(460–550aa)-mEGFP failed to condense (*SI Appendix*, Fig. S2 *D* and *E*), whereas IDR2-Δ(323–442aa)-mEGFP protein formed spherical condensates in vitro, which was affected by protein concentration and salt content with similarity to IDR2-mEGFP (*SI Appendix*, Fig. S2 *E* and *F*). Further, we tried to narrow down the region within 460–550aa that was required for the LLPS of RNF168. However, all of the smaller deletion within 460–550aa, including Δ(466–478aa) (that is ΔLRM2), Δ479–550aa, Δ(460–504aa), and Δ(505–550aa), could not abolish the LLPS of RNF168 (Fig. 2*H*). Moreover, purified (460–550aa)-mEGFP formed condensates in vitro, while its fragment (479–550aa)-mEGFP formed remarkably smaller and fewer condensates, and LRM2-mEGFP failed to condense (*SI Appendix*, Fig. S2 *G* and *H*). Together, the 460–550aa is the dominant disordered region required for the LLPS of RNF168.

**K63-Linked Polyubiquitin Chains Enhance the LLPS of RNF168.** As shown, endogenous RNF168 hardly condensed due to its relatively low expression but rapidly formed liquid-like puncta at DSB sites after irradiation (Fig. 1*D*). Next, we asked how it was induced at DSB sites. Apart from IDR-driven interactions, multivalent interactions among different biomolecules also contribute to LLPS. Previous studies had revealed that RNF168

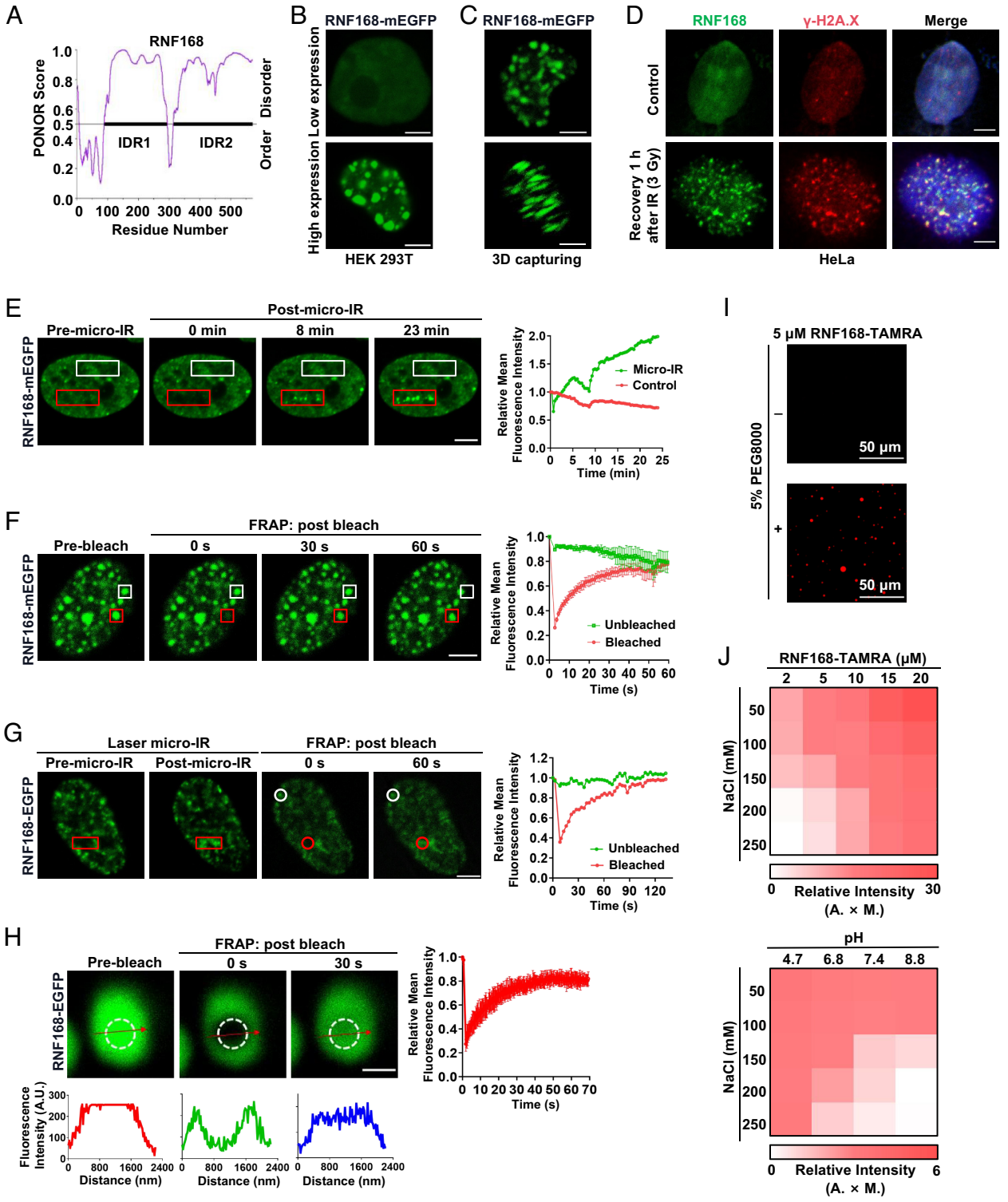


**Fig. 1.** RNF168 forms liquid-like condensates at DNA damage sites. (*A*) Disordered region analysis of RNF168 using PONDR (http://www.pondr.com). (*B*) Representative images of exogenous RNF168-mEGFP in HEK 293T cells transfected with low (0.3 μg) or high (1 μg) dose of plasmid for 24 h. (*C*) 3D-capturing images of RNF168-mEGFP condensates in HEK 293T cells transfected with plasmid. (*D*) The IF assay was performed to detect the endogenous RNF168 and γ-H2A.X signals after 1 h recovery from irradiation (3 Gy) in HeLa cells. RNF168 formed puncta colocalized with γ-H2A.X in the nucleus. (*E*) Exogenous RNF168-mEGFP formed spherical puncta in the microirradiated region of which fluorescence intensity increased over time in HeLa cells. (*F*) FRAP assay of exogenous RNF168-mEGFP puncta in HeLa cells. (*G*) FRAP assay of microirradiation induced RNF168-EGFP puncta in HeLa cells. (*H*) The FRAP assay was performed within an RNF168-EGFP condensate in cells. (*I*) TAMRA-dyed RNF168 protein formed condensates in buffers containing 20 mM Tris-HCl (pH 7.4), 150 mM NaCl, and 5% PEG8000 visualized by confocal microscopy. (*J*) The impacts of protein concentration, salt content, and pH on RNF168 condensation in vitro. The fluorescence intensities of condensates were presented as the area × mean intensity (A. × M.). Data were presented as mean ± SEM (Scale bar, 5 μm) (unless otherwise specified in the image).

recognized ubiquitinated H1 and functioned as an E3 ligase for H2A.X ubiquitination at DSB sites (6), while polyubiquitin has been found to enhance LLPS of proteins (22, 29). We therefore hypothesized that the interaction between RNF168 and ubiquitinated histone might trigger its LLPS at DSB sites. In vitro assays showed that high concentration of purified RNF168 protein

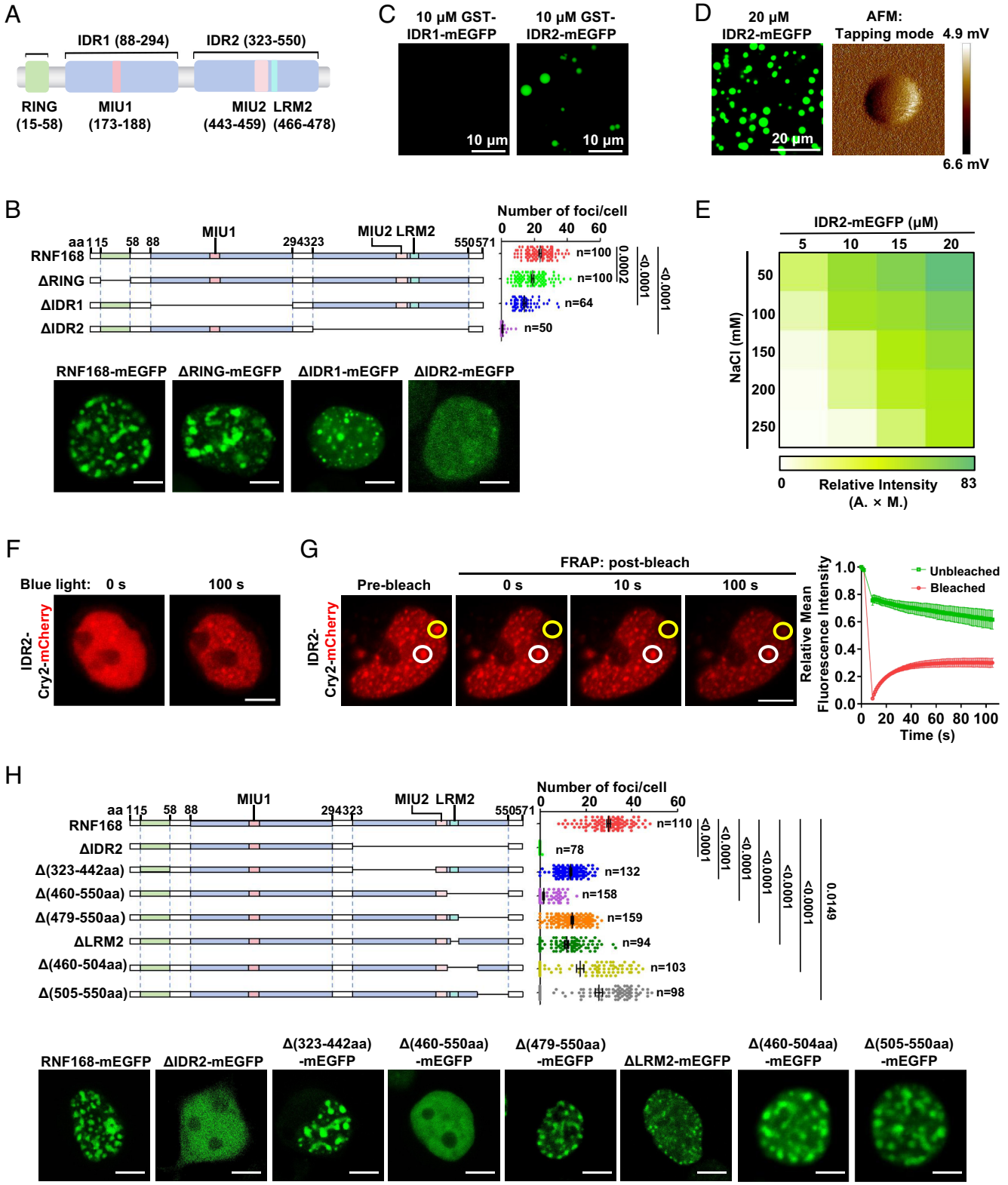


**Fig. 2.** Disordered region 460–550aa is essential for the LLPS of RNF168. (*A*) Schematic diagram of RNF168 consisting of a RING domain and two IDRs (IDR1 and IDR2). IDR1 contains an MIU1, while IDR2 contains an MIU2 and a LRM2 motif, respectively. (*B*) Schematic diagram and representative images of mEGFP-tagged RNF168, ΔRING, ΔIDR1, and ΔIDR2 mutants in HEK 293T cells transfected with indicated plasmids. Counts of RNF168 puncta per cell were shown. (*C*) In vitro condensation assay of purified recombinant GST-IDR1-mEGFP and GST-IDR2-mEGFP protein. 10 μM IDR2-mEGFP protein formed spherical condensates in buffers containing 20 mM Tris-HCl (pH 7.4), 150 mM NaCl, and 5% PEG8000. (*D*) 20 μM IDR2-mEGFP condensates showed round and smooth surface captured by AFM under the same buffer condition to (*C*). (*E*) The impacts of protein concentration and salt content on condensation of IDR2-mEGFP protein. The fluorescence intensities were presented as the area × mean intensity (A. × M.). (*F*) Exogenous IDR2-Cry2-mCherry formed puncta at stimulation of blue light (488 nm) in HEK 293T cells. (*G*) FRAP assay of the blue light-induced IDR2-Cry2-mCherry puncta in HEK 293T cells. (*H*) Schematic diagram and representative images of mEGFP-tagged RNF168, ΔIDR2, Δ(323–442aa), Δ(460–550aa), Δ(479–550aa), ΔLRM2, Δ(460–504aa), and Δ(505–550aa) mutants in HEK 293T cells. Counts of RNF168 puncta per cell were shown. Data were presented as mean ± SEM (Scale bar, 5 μm) (unless otherwise specified in the image).

underwent LLPS without PEG8000, while Δ(460–550aa) protein remained diffused (Fig. 3 *A* and *B*). In a buffer with higher salt concentration (210 mM NaCl), neither RNF168 nor Δ(460–550aa) formed visible puncta (Fig. 3 *C*, *Top* panel). Importantly, addition of K63-linked polyubiquitin chains remarkably induced LLPS of RNF168 protein, which spread and fused as oil-like condensates when time increased (Fig. 3 *C*, *Left* panel). Though Δ(460–550aa) tended to form puncta when incubated with

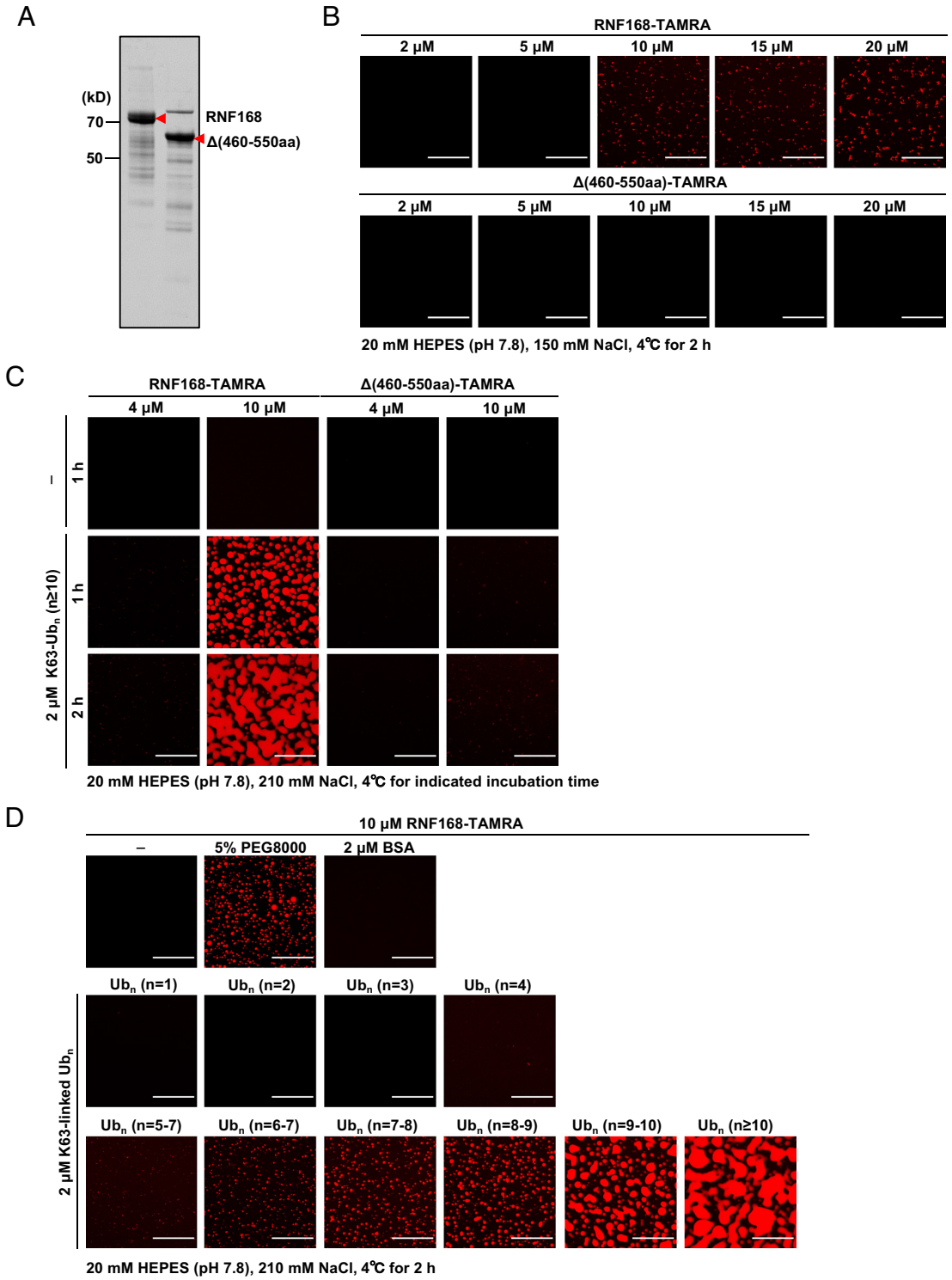


**Fig. 3.** K63-linked polyubiquitin chains enhance the LLPS of RNF168. (*A*) Coomassie blue staining of purified RNF168 and Δ(460–550aa) proteins. (*B*) In vitro condensation assay of TAMRA-dyed RNF168 and Δ(460–550aa) proteins under distinct concentrations in buffers containing 20 mM HEPES (pH 7.8) and 150 mM NaCl. The mixture reacted at 4 °C for 2 h before observation. (*C*) In vitro condensation assay of TAMRA-dyed RNF168 and Δ(460–550aa) proteins with or without K63-linked polyubiquitin chains. Note that TAMRA-dyed RNF168 protein hardly formed condensates in high salt condition (210 mM NaCl). Addition of 2 μM K63-linked polyubiquitin chains (linkage length n ≥ 10) significantly promoted RNF168 to form liquid-like condensates under high protein concentration (10 μM). The polyubiquitin-induced RNF168 condensates enlarged over time. Comparatively, polyubiquitin only slightly induced Δ(460–550aa) to form small puncta albeit with high protein concentration (10 μM). (*D*) The impacts of K63-linked ubiquitin chains with distinct linkage lengths on the condensation of 10 μM TAMRA-dyed RNF168 proteins in buffers containing 20 mM HEPES (pH 7.8) and 210 mM NaCl. The mixture was incubated at 4 °C for 2 h before observation (Scale bar, 50 μm) (unless otherwise specified in the image).

polyubiquitin, it was much weaker than full-length RNF168 (Fig. 3 *C*, *Right* panel). Comparatively, K48-linked polyubiquitin induced RNF168 condensation but it was far less than that of K63-linked polyubiquitin (*SI Appendix*, Fig. S3*A*). Considering that polyubiquitin chains of different polymers provide varieties in multivalency, we incubated RNF168 protein with mono- or polyubiquitin (*SI Appendix*, Fig. S3*B*) and found that the larger polymer of ubiquitin induced stronger RNF168 condensation (Fig. 3*D*). These in vitro findings suggest that interacting with polyubiquitin or ubiquitinated substrates might trigger LLPS of RNF168 at DSB sites.

**LLPS Is Required for the Recruitment of RNF168 and It-Mediated H2A.X Ubiquitination.** Next, we asked whether and how LLPS functioned in RNF168-mediated DSB repair. To perform the loss-of-function assay, Δ(460–550aa) was used as a mutant of RNF168 without LLPS capacity. As shown, exogenous Δ(460–550aa)-mEGFP accumulated much less and slower at laser-irradiated regions than RNF168-mEGFP, which was independent of endogenous RNF168 (Fig. 4*A* and *SI Appendix*, Fig. S4*A*). A similar finding was observed in RNF168-knockout (KO) HeLa cells stably re-expressing sgRNA-resistant RNF168 and Δ(460–550aa) upon X-ray irradiation. The localization of Δ(460–550aa) mutant in DNA lesions (indicated as γ-H2A.X signals) was apparently attenuated throughout the DNA damage repair process (Fig. 4*B*). As the accumulation of RNF168 is required for H2A.X ubiquitination, we assumed that the LLPS deficiency of RNF168 might further suppress its catalytic activity. Indeed, irradiation-induced ubiquitinated H2A.X was decreased in RNF168-KO HeLa cells (Fig. 4 *C*, *Left* panel). Re-expressing RNF168-mEGFP in RNF168-KO cells recovered the H2A.X ubiquitination, while LLPS-deficient Δ(460–550aa)-mEGFP-expressing cells performed similarly to the control cells (Fig. 4 *C*, *Right* panel). The immunofluorescence (IF) assay also showed that ubiquitination at DSB sites depended on the LLPS of RNF168 (Fig. 4*D* and *SI Appendix*, Fig. S4*B*). Consistently, continuously treated by a lower dose of 1,6-hexanediol (2.5%) prior to irradiation significantly impaired RNF168-mediated ubiquitination at DSB sites (Fig. 4*E*). Disrupting LLPS by treating with a higher dose of 1,6-hexanediol (8 to 10%) after irradiation also dissolved the RNF168-dependent ubiquitinated products (*SI Appendix*, Fig. S4*C*). Therefore, LLPS is required for the accumulation of RNF168 at DSB sites and it-mediated H2A.X ubiquitination.

Given that ubiquitination of H2A.X provides a binding platform for downstream repair factors, we further investigated whether LLPS deficiency of RNF168 inhibited this phenotype. Recruitment of BRCA1 and 53BP1 to irradiation-induced damaged DNA were remarkably blocked in RNF168-KO or RNF168-KD HeLa cells (Fig. 4 *F* and *G* and *SI Appendix*, Fig. S4 *D* and *E*). Re-expression of RNF168 rescued the accumulation of BRCA1 and 53BP1, whereas Δ(460–550aa) failed to recruit the downstream factors (Fig. 4 *F* and *G* and *SI Appendix*, Fig. S4 *D* and *E*). These findings further confirm that RNF168 accumulates at DSB sites and ubiquitylates H2A.X in a LLPS-dependent manner.

**LLPS of RNF168 Promotes DSB Repair.** Previous studies revealed that a LR motif named LRM2 (466–478aa) is essential for RNF168 binding to the nucleosome during DSB repair (30). In our study, LRM2 was found to be an important disordered fragment driving RNF168 LLPS, for recovering LRM2 in Δ(460–550aa) [designated as Δ(479–550aa)] apparently regained the foci formation (Fig. 2*H*). Therefore, we constructed an artificial mutant supplementing a LRM2 motif at the C-terminal of Δ(460–550aa), designated as Δ(460–550aa)-LRM2, to retain the capacity of nucleosome binding under LLPS deficiency (Fig. 5 *A* and *B*). Consistent with previous reports (30), deletion of MIU2 or LRM2 reduced the ubiquitination signals at DSB sites and subsequent 53BP1 recruitment (Fig. 5 *C* and *D* and *SI Appendix*, Fig. S5 *A* and *B*). Specifically, Δ(460–550aa)-LRM2-expressing cells showed a higher level of substrates ubiquitination and 53BP1 accumulation than that of Δ(460–550aa) mutant loss of LRM2 function (Fig. 5 *C* and *D* and *SI Appendix*, Fig. S5 *A* and *B*). Yet, compared to full-length RNF168, either Δ(460–550aa) or Δ(460–550aa)-LRM2 showed remarkable attenuation in the irradiation-induced signals mentioned above (Fig. 5 *C* and *D* and *SI Appendix*, Fig. S5 *A* and *B*). Similar to the DNA repair defect of RNF168 deletion (*SI Appendix*, Fig. S5 *C* and *D*), LLPS deficiency [Δ(460–550aa) or Δ(460–550aa)-LRM2] also resulted in a delayed DSB repair (Fig. 5 *E* and *F*).

To further verify the important role of LLPS in RNF168-mediated DSB repair, we fused two tandem N-terminal IDR of fused in sarcoma (FUSN, 1–214aa), an RNA-binding protein with recognized LLPS property (31), to the C-terminal of the Δ(460–550aa)-LRM2 mutant, designated as Δ(460–550aa)-LRM2-$(FUSN)_2$, to restore its LLPS function (Fig. 5*G*). Indeed, the clearance of γ-H2A.X was faster in Δ(460–550aa)-LRM2-$(FUSN)_2$-expressing cells than (460-550aa)-LRM2, indicating that fusion of $(FUSN)_2$ restored LLPS and the DSB repair capacity of Δ(460–550aa)-LRM2 (Fig. 5*H*). In addition, an optogenetic system, "Corelets" (32), was introduced to restore the LLPS function of the Δ(460–550aa)-LRM2 mutant under blue light activation (*SI Appendix*, Fig. S6 *A–C*). Along with the light-activated LLPS, Δ(460–550aa)-LRM2 showed an accelerated accumulation at DNA damage sites (*SI Appendix*, Fig. S6 *D–F*). These gain-of-function assays supported the essential role of LLPS in promoting RNF168-mediated DSB repair. Furthermore, LLPS-deficient RNF168 [Δ(460–550aa) or Δ(460–550aa)-LRM2] showed a significant reduction in direct interactions with downstream factors, including 53BP1 and BRCA1 (Fig. 6 *A* and *B*).

Together, our finding confirms that in the context of ubiquitin or nucleosome binding function, LLPS of RNF168 promotes it-mediated DSB repair by accelerating its accumulation at DSB sites, enhancing RNF168-catalyzed H2A.X ubiquitination and recruiting downstream factors including 53BP1 and BRCA1 (Fig. 6*C*).

## Discussion

In the current study, we show that RNF168 condensation at DSB lesions is a process of LLPS, which is driven by the IDR domain (460–550aa) and enhanced by the interaction with K63-linked polyubiquitin chains. RNF168 condensation accelerates its accumulation at DSBs and enhances it-mediated H2A.X ubiquitination, which might further promote its condensation in a positive feedback manner. Moreover, RNF168 condensation is required for the accumulation of 53BP1 and BRCA1 to DSBs which finally promote the DSB repair (Fig. 6*C*). The study provides a mechanism for spatiotemporal regulation in DSB response.

The association and disassociation of DNA repair factors at DSB lesions have been observed for decades (33, 34), which are recently found to be similar to the dynamic exchange between condensates and surroundings (35). Indeed, we and other groups have identified several DSB repair factors undergoing LLPS, which participate in different stages of DSB response (21, 22, 25). In the initial stage, MRNIP condensates recruit MRN complex and cluster DSBs to facilitate DSB sensing and ATM activation (21); PAR provides a scaffold for DNA repair factors and seeds a liquid-like repair center (24). For NHEJ-mediated DSB repair,

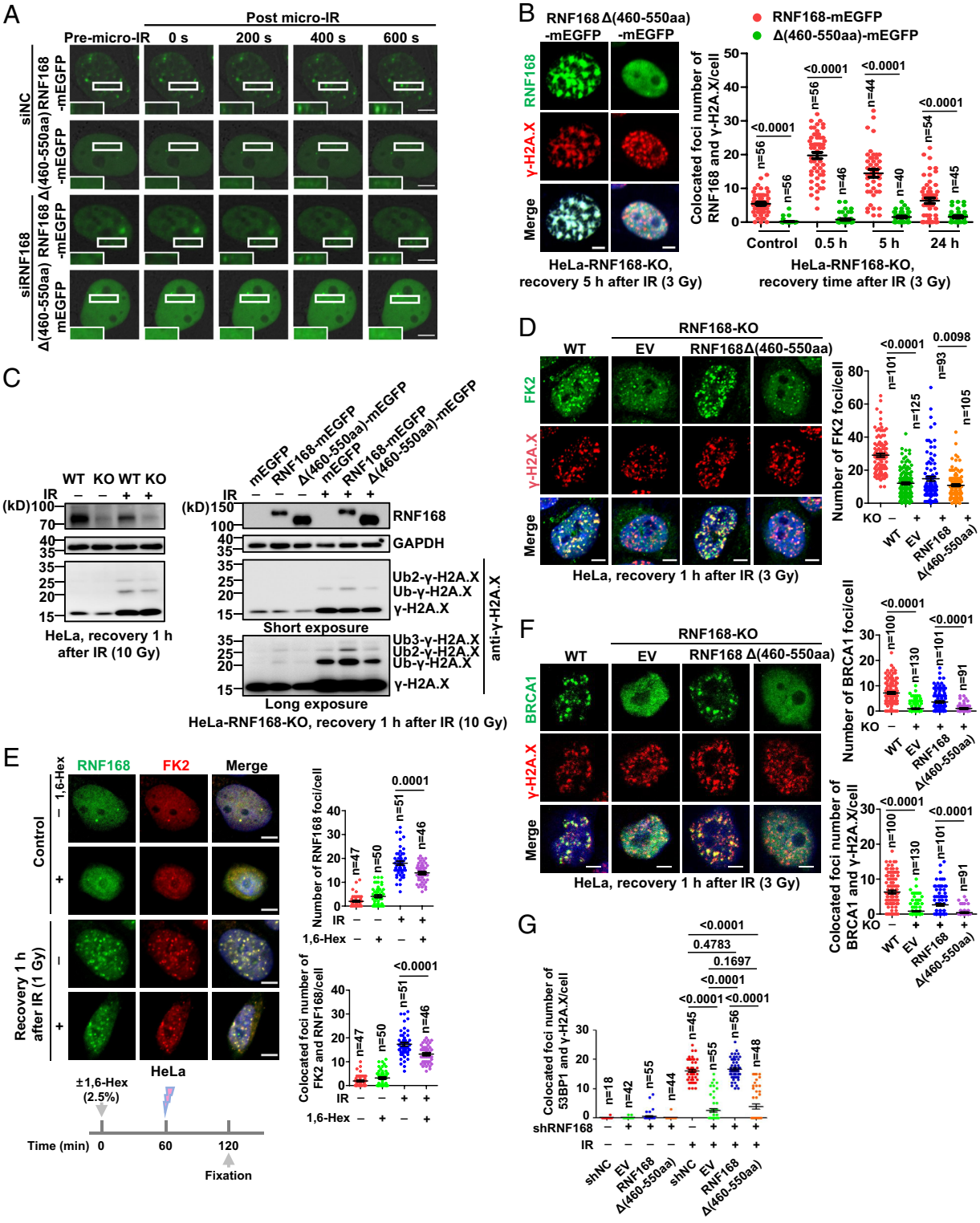


**Fig. 4.** LLPS is required for the recruitment of RNF168 and it-mediated H2A.X ubiquitination. (*A*) The laser microirradiation assay was performed to explore the impacts of IDR deletion on RNF168 recruitment at DSB sites. Where indicated, HeLa cells were transfected with siNC or siRNF168 for 48 h before microirradiation. Note that exogenous RNF168-mEGFP formed spherical condensates in the microirradiated region, while Δ(460–550aa)-mEGFP displayed ground-glass assembly, independent of endogenous RNF168. (*B*) The IF assay was performed to explore the impacts of IDR deletion on RNF168 recruitment at DSB sites. IF of RNF168 and γ-H2A.X was detected at 0, 0.5, 5, and 24 h after 3 Gy irradiation, and the numbers of colocalized foci were counted. Representative images of cells at 5 h after irradiation were presented. (*C*) Western blotting showed the impacts of IDR deletion on RNF168-mediated H2A.X ubiquitination. The levels of H2A.X ubiquitination were detected by anti-γ-H2A.X antibody at 1 h after 10 Gy irradiation. For (*B* and *C*), RNF168-KO HeLa cells stably re-expressing mEGFP or sgRNA-resistant RNF168 variants were used. (*D*) The IF assay was performed to explore the impacts of IDR deletion on RNF168-mediated ubiquitinated conjugates at DSB sites. IF of ubiquitinated conjugates (detected by anti-FK2) and γ-H2A.X was detected at 1 h after 3 Gy irradiation, and the numbers of FK2 foci were counted. (*E*) HeLa cells transfected with RNF168-mEGFP plasmid for 48 h were continuously treated with 2.5% 1,6-hexanediol from 1 h before irradiation till 1 h after irradiation (1 Gy). Cells were then fixed and subjected to the IF assay. The numbers of exogenous RNF168 foci as well as the colocalized foci of RNF168 and FK2 were counted. (*F* and *G*) IF assays were performed to explore the impacts of LLPS deficiency of RNF168 on BRCA1 (*F*) and 53BP1 (*G*) recruitment at DSB sites. IF of BRCA1, 53BP1, and γ-H2A.X was detected at 1 h after 3 Gy irradiation. For (*D*, *F*, and *G*), RNF168-KO or RNF168-knockdown (KD) HeLa cells stably re-expressing sgRNA- or shRNA-resistant RNF168 variants were used. Data were presented as mean ± SEM (Scale bar, 5 μm) (unless otherwise specified in the image).

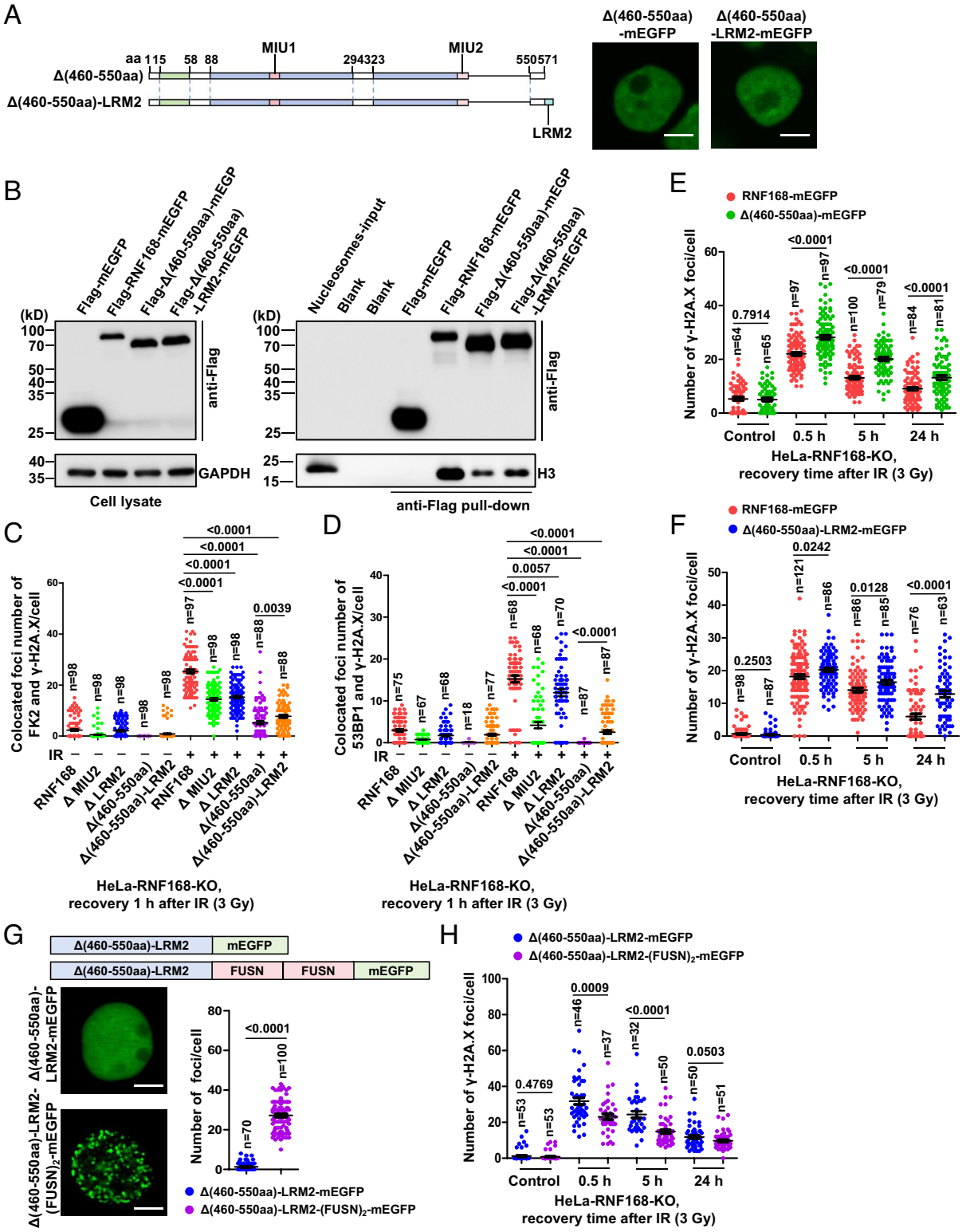


**Fig. 5.** LLPS of RNF168 promotes DSB repair. (*A*) Schematic diagram and representative images of Δ(460–550aa) and Δ(460–550aa)-LRM2 in HEK 293T transfected with indicated plasmids. (*B*) Flag-tagged protein/nucleosomes pull-down assay to verify the nucleosome binding capacity of RNF168 variants. HEK 293T cells were transfected with Flag-tagged RNF168, Δ(460–550aa), or Δ(460–550aa)-LRM2 plasmids for 48 h before cell lysis. The lysates were incubated with cell-derived nucleosomes, and the pull-downs were analyzed by western blotting. Nucleosomes were indicated by anti-H3. (*C* and *D*) The IF assay was performed to explore the impacts on ubiquitination (*C*) and 53BP1 recruitment (*D*) at DSB sites of distinct mutants including ΔMIU2, ΔLRM2, Δ(460–550aa), and Δ(460–550aa)-LRM2. IF of FK2, 53BP1, and γ-H2A.X was detected at 1 h after 3 Gy irradiation. Numbers of colocalized foci were counted. (*E* and *F*) The IF assay was performed to analyze the impacts on the DNA damage response process of Δ(460–550aa) (*E*) and Δ(460-550aa)-LRM2 (*F*). IF of γ-H2A.X was detected at distinct time points after 3 Gy irradiation. (*G*) Representative images of mEGFP-tagged Δ(460–550aa)-LRM2 and Δ(460–550aa)-LRM2-$(FUSN)_2$ in HEK 293T cells transfected with indicated plasmids. Counts of RNF168 puncta per cell were shown. (*H*) The IF assay was performed to analyze whether regaining LLPS function by FUSN fusion rescued the DSB repair defect of the Δ(460–550aa)-LRM2 mutant. IF of γ-H2A.X was detected at distinct time points after 3 Gy irradiation. Data were presented as mean ± SEM (Scale bar, 5 μm) (unless otherwise specified in the image).

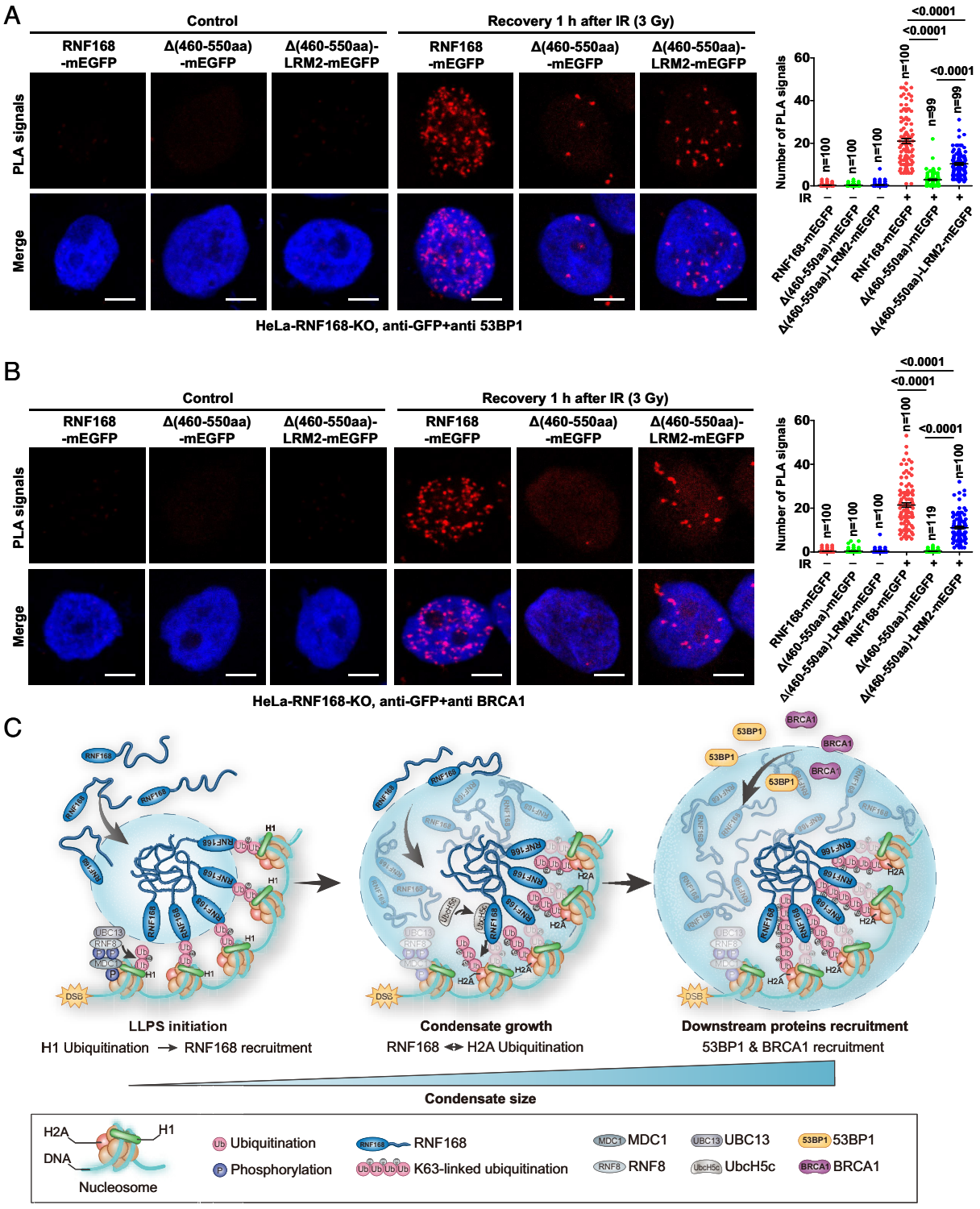


**Fig. 6.** LLPS promotes RNF168 interacting with 53BP1 and BRCA1 at DSB sites. (*A* and *B*) The proximity ligation assay (PLA) was performed to verify the impacts of LLPS on the interactions between RNF168 and downstream factor 53BP1 (*A*) or BRCA1 (*B*) using the RNF168-KO HeLa cells stably re-expressing mEGFP-tagged wild-type or mutant RNF168. The PLA signals were detected by anti-GFP, anti-53BP1 and anti-BRCA1. (*C*) Schematic diagram for ubiquitin-induced RNF168 condensation promoting DNA DSB repair. In the initial stage of DSB repair, RNF168 assembles at DSB sites via binding to ubiquitinated H1 catalyzed by RNF8 and undergoes LLPS in a self-interacting IDR-driven manner. RNF168 subsequently triggers and amplifies the ubiquitination of H2A.X, which provides multivalent interactions and further enhances RNF168 condensation. This positive feedback axis drives the rapid accumulation of RNF168 at DSB sites and the subsequent recruitment of downstream repair factors (53BP1 and BRCA1) for DSB repair. Data were presented as mean ± SEM (Scale bar, 5 μm) (unless otherwise specified in the image).

53BP1 is recruited to DSBs by dilncRNAs to form liquid-like condensates, further promoting DSB repair and p53 activation (25, 27). In *Saccharomyces cerevisiae*, cooperation between Rad52 condensates and various types of nuclear filaments promotes the DNA repair center assembly and maintains the genome stability (36). Here, we identified RNF168, an essential DSB repair factor, underwent LLPS at DSB lesions to accelerate its accumulation and it-mediated ubiquitination of H2A.X. Deletion of the

LLPS-driving domain remarkably attenuated RNF168-mediated H2A.X ubiquitination and therefore impaired downstream 53BP1 and BRCA1 binding to the scaffold ubiquitinated H2A.X. More importantly, restoring the LLPS property of Δ(460–550aa)-LRM2 mutant by either fusing with the FUSN (a well-characterized IDR) or using the optogenetic system Corelets successfully rescued the DSB repair defect. Therefore, our results further support the important role of LLPS in the initiation stage of DSB repair to recruit key repair factors.

It is demonstrated that LLPS is enhanced by multivalent association, which may be provided by scaffold molecules (37). Many types of such scaffold molecules have been identified, including nucleic acids, PAR, and polyubiquitin chains (24, 37–40). For example, exogenous double-strand DNA in cytoplasm remarkably induces the condensation of cyclic GMP-AMP synthase (cGAS), a DNA-binding protein essential for innate immune activation (39). Polyubiquitin-involved LLPS functions in various biological processes. Multivalent interactions between RAD23B and K48-linked polyubiquitin chains induce the LLPS of proteasome to regulate proteostasis (40). Autophagy adaptor p62 undergoes phase separation in a K63-linked polyubiquitin chain-dependent manner which further drives autophagosomes' concentration and segregation (29). In the DSB repair process, RNA and PAR have been reported to function as the inducers for DSB repair factor condensation (24, 41), such as 53BP1/dilncRNAs (25, 27) and FUS/PAR (42). However, as a key player in DSB repair, whether DSB-induced ubiquitination on histone functions as a LLPS stimulator of DSB repair factors remains unclear. Our data suggest that in addition to recruiting DSB repair proteins by direct interaction, polyubiquitin chains also promote DSB repair by inducing LLPS of RNF168.

We report that RNF168 condensation accelerates its accumulation and it-dependent H2A.X ubiquitination at DSB lesions. The mechanism of RNF168 recruitment to DSB sites has been studied for a decade. Doil et al. first showed that RNF168 assembled at DSBs in an RNF8-dependent manner and amplified K63-linked ubiquitin conjugates at H2A and H2A.X which were required for retention of 53BP1 and BRCA1 (14, 43). Later, H1, instead of H2A, was identified as the RNF8-catalyzed substrate at DSB lesions upon the coupling of UBC13 (6). In this study, RNF168 recruitment was found to be dependent on the physical binding between its ubiquitin-dependent module (UDM) and K63-ubiquitinated H1 (6). Here, our results reveal a possible mechanism that after the recruitment by K63-ubiquitinated H1, RNF168 further undergoes LLPS under the stimulation of K63-linked ubiquitin chains. This process facilitates RNF168 accumulation at DSBs to catalyze the ubiquitination of H2A.X, which binds RNF168 with high multivalency and thereby enhances RNF168 condensation in a positive feedback manner. This positive feedback axis may drive the rapid accumulation of RNF168 at DSBs and subsequent signal transduction of DSB repair (Fig. 6*C*).

Interestingly, a recent study found that SUMOylated RNF168 underwent LLPS to form nuclear condensates, while upon DNA damage, RNF168 LLPS was diminished and released from condensates to participate in DSB repair (44). Their conclusion was very different from our finding that LLPS promoted RNF168-mediated DSB repair. We proposed the inconsistency might be due to the variation between cell lines. In the cell lines we used, spontaneous RNF168 condensates were very rare in unirradiated cells, thereby we focused on the irradiation-induced RNF168 condensates. Although Wei et al. proposed that RNF168 formed condensates in cells without DNA damage, some cell lines, including HCT116 and HEK 293T, presented very rare condensates forming by endogenous RNF168 in their paper (their Fig. 5 *E* and *F*). Otherwise, we noticed that several important data were consistent between Wei et al. and our study: First and most importantly, RNF168 had the potential to undergo LLPS participating in DNA damage repair; second, RNF168 condensates recruited 53BP1; and third, purified RNF168 protein at low concentration hardly underwent LLPS without stimulators in vitro. In our opinion, these two studies propose a model of RNF168 LLPS function in DSB repair: In context of physiological condition, RNF168 is SUMOylated and forms condensates to keep away from chromatin; upon DSB occurs, RNF168 is deSUMOylated, released from condensates and recruited to DSB lesions, where polyubiquitin stimulates RNF168 undergoing LLPS to facilitate it-mediated H2A.X ubiquitination and 53BP1 recruitment, thereby promoting DSB repair.

Together, our study uncovers a mechanism that IDR-driven and polyubiquitin-enhanced LLPS promotes RNF168 accumulation at damaged DNA and related DNA repair function, supporting the important role of LLPS in DNA damage response.

## Materials and Methods

**Live-Cell Imaging.** HEK 293T or HeLa cells were plated in glass-bottom dishes and transfected with indicated plasmids for 24 h before observation. Nuclear were stained using Hoechst 33342 (4082, CST, Danvers, MA) at a final concentration of 1 μg/mL for 10 min. Live-cell images were obtained using a Zeiss LSM880 confocal microscope where cells were kept in an incubation chamber at 37 °C with 5% $CO_2$.

***FRAP.*** The FRAP assays were conducted as previously described (21, 45). Puncta were entirely or partly photobleached by 488 or 561 nm laser under 100% power followed by a time-series imaging (time interval of 1 s). Fluorescence intensities of the photobleached region and adjacent control region were measured using ZEN software (Blue edition, 3.1).

***Laser microirradiation.*** HeLa cells were presensitized with 10 μM BrdU and transfected with EGFP or mEGFP-tagged plasmids for 24 h prior to microirradiation. Line-like regions were selected and microirradiated by 405 nm laser. The ZEN software (Blue edition, 3.1) was used to quantify the fluorescence intensities of the laser stripes. The laser microirradiation protocol was performed as previously described (46).

***OptoIDR assay.*** The optoIDR assay was conducted as previously described (28). HEK 293 T cells transfected with IDR2-Cry2-mCherry plasmids for 24 h were exposed to blue light pulses (488 nm, time interval of 2 s) under 50% laser power during a time-series imaging (time interval of 1 s). FRAP and 1,6-hexanediol treatment on the photoinduced condensates were performed and imaged every 1 s with blue light off.

***Corelets optogenetic system.*** The Corelets system was activated according to the protocol previously described (32). HEK 293T cells were cotransfected with NLS-iLID-EGFP-FTH1 and indicated IDR-mCherry-SspB plasmids for 48 h before imaging. Considering the overlap between the EGFP excitation (488 nm) and iLID activation spectrum, the preactivation imaging was captured by the mCherry channel only (561 nm). For Corelets activation, cells were continuously imaged by the dual channel (561 and 488 nm) to capture both the FTH1 core and IDR component.

**In Vitro Condensation Assay.** The TAMRA-labeled RNF168 or recombinant IDR-mEGFP proteins were adjusted to indicated concentrations in various buffer conditions (20 mM Tris-HCl or HEPES of indicated pH with different salt content) for the in vitro condensation assay. Each reaction was incubated in the 384-well glass-bottom plate (P384-1.5H-N, Cellvis, Sunnyvale, CA) at room temperature or at 4 °C for the indicated time before observation. Images were captured using a Zeiss LSM880 confocal microscope and further processed by ZEN software (Blue edition, 3.1).

**Flag-Tagged Protein/Nucleosomes Pull-Down Assay.** HEK 293T cells were transfected with indicated Flag-tagged constructs for 48 h and lysed in IP lysis buffer [25 mM Tris-HCl (pH 7.5), 150 mM NaCl, 1% NP-40, 1 mM EDTA, 5% (v/v) glycerol, and 1 × protease inhibitor]. Cell lysates were incubated with Flag-beads for 2 h at 4 °C. The mixture was then washed five times in the IP lysis buffer and incubated with 2 μg nucleosomes for 1 h at 4 °C. After five times washes in IP lysis buffer, the pull-down Flag-tagged protein/nucleosomes were finally

eluted by 0.1 M glycine (pH 3.0) and neutralized by 2.5 M NaOH before western blotting analysis.

Detailed methods on cell culture, plasmid and cell line construction, protein expression and purification, nucleosomes isolation, western blotting, IF assay, PLA, 1,6-hexanediol treatment, atomic force microscope imaging, and statistical analysis are available in *SI Appendix, Materials and Methods*.

**Data, Materials, and Software Availability.** All study data are included in the article and/or supporting information.

**ACKNOWLEDGMENTS.** We are thankful for the professional suggestions and technological support from Prof. Lei Liu (Department of Chemistry, Tsinghua University), as well as Prof. Pi-Long Li and Dr. Yu-Xuan Jiang (School of Life Sciences, Tsinghua University). Research funding was provided by the National Key Research and Development Program of China (Nos. 2022YFC2503700 and 2022YFA1105300); National Science Fund for Distinguished Young Scholars (No. 82225040); National Science Fund for Excellent Young Scholars (No. 82122057); Natural Science Foundation of China (Nos. 82103770, 82171163, 82302307, and 82373513); Science Fund for Distinguished Young Scholars of Guangdong Province (No. 2021B1515020022); Guangdong Science and Technology Project (No. 2022A1515012363); Beijing Bethune Charitable Foundation (No. flzh202102); Fundamental Research Funds for the Central Universities (No. 22qntd3602); National Postdoctoral Program for Innovative Talents of China (No. BX20220359); National Science and Technology Council Taiwan (NSTC 112-2639-B-039-001-ASP and T-star Center NSTC 113-2634-F-039-001-); Ministry of Health and Welfare Taiwan (MOHW113-TDU-B-222-134016); and The Featured Areas Research Center Program by the Ministry of Education in Taiwan.

Author affiliations: [a]Department of Pathology, Henan Provincial Key Laboratory of Radiation Medicine, The First Affiliated Hospital of Zhengzhou University, Zhengzhou, Henan 450052, China; [b]Tianjian Laboratory of Advanced Biomedical Sciences, Zhengzhou University, Zhengzhou, Henan 450052, China; [c]State Key Laboratory of Oncology in South China, Collaborative Innovation Center for Cancer Medicine, Sun Yat-sen University Cancer Center, Guangzhou, Guangdong 510060, China; [d]Department of Radiology, Sun Yat-sen University Cancer Center, Guangzhou, Guangdong 510060, China; [e]Guangdong Provincial Key Laboratory of Colorectal and Pelvic Floor Diseases, The Sixth Affiliated Hospital of Sun Yat-sen University, Guangzhou, Guangdong 510655, China; [f]Tsinghua-Peking Joint Center for Life Sciences, Ministry of Education Key Laboratory of Bioorganic Phosphorus Chemistry and Chemical Biology, Department of Chemistry, Tsinghua University, Beijing 100084, China; [g]Department of Radiation Oncology, The Sixth Affiliated Hospital of Sun Yat-sen University, Guangzhou, Guangdong 510655, China; [h]Biomedical Innovation Center, The Sixth Affiliated Hospital, Sun Yat-sen University, Guangzhou, Guangdong 510655, China; [i]Department of Radiation Oncology, The First Affiliated Hospital of Zhengzhou University, Zhengzhou, Henan 450052, China; [j]Academy of Medical Sciences, Zhengzhou University, Zhengzhou, Henan 450052, China; and [k]Graduate Institute of Biomedical Sciences, Institute of Biochemistry and Molecular Biology, Research Center for Cancer Biology, Cancer Biology and Precision Therapeutics Center, and Center for Molecular Medicine, China Medical University, Taichung 406, Taiwan (Republic of China)

1. R. Scully, A. Panday, R. Elango, N. A. Willis, DNA double-strand break repair-pathway choice in somatic mammalian cells. *Nat. Rev. Mol. Cell Biol.* **20**, 698–714 (2019).
2. S. Parmar, H. Easwaran, Genetic and epigenetic dependencies in colorectal cancer development. *Gastroenterol. Rep.* **10**, goac035 (2022).
3. A. Celeste *et al.*, Histone H2AX phosphorylation is dispensable for the initial recognition of DNA breaks. *Nat. Cell Biol.* **5**, 675–679 (2003).
4. M. Lavin, S. Kozlov, M. Gatei, A. Kijas, ATM-dependent phosphorylation of all three members of the MRN complex: From sensor to adaptor. *Biomolecules* **5**, 2877–2902 (2015).
5. Z. Wang *et al.*, MRE11 UFMylation promotes ATM activation. *Nucleic Acids Res.* **47**, 4124–4135 (2019).
6. T. Thorslund *et al.*, Histone H1 couples initiation and amplification of ubiquitin signalling after DNA damage. *Nature* **527**, 389–393 (2015).
7. F. Mattiroli *et al.*, RNF168 ubiquitinates K13–15 on H2A/H2AX to drive DNA damage signaling. *Cell* **150**, 1182–1195 (2012).
8. V. Horn *et al.*, Structural basis of specific H2A K13/K15 ubiquitination by RNF168. *Nat. Commun.* **10**, 1751 (2019).
9. A. Fradet-Turcotte *et al.*, 53BP1 is a reader of the DNA-damage-induced H2A Lys 15 ubiquitin mark. *Nature* **499**, 50–54 (2013).
10. J. R. Becker *et al.*, BARD1 reads H2A lysine 15 ubiquitination to direct homologous recombination. *Nature* **596**, 433–437 (2021).
11. B. Zhao, E. Rothenberg, D. A. Ramsden, M. R. Lieber, The molecular basis and disease relevance of non-homologous DNA end joining. *Nat. Rev. Mol. Cell Biol.* **21**, 765–781 (2020).
12. X. Li, W.-D. Heyer, Homologous recombination in DNA repair and DNA damage tolerance. *Cell Res.* **18**, 99–113 (2008).
13. J. A. Schmid *et al.*, Histone ubiquitination by the DNA damage response is required for efficient DNA replication in unperturbed S phase. *Mol. Cell* **71**, 897–910.e8 (2018).
14. G. S. Stewart *et al.*, The RIDDLE syndrome protein mediates a ubiquitin-dependent signaling cascade at sites of DNA damage. *Cell* **136**, 420–434 (2009).
15. G. S. Stewart *et al.*, RIDDLE immunodeficiency syndrome is linked to defects in 53BP1-mediated DNA damage signaling. *Proc. Natl. Acad. Sci. U.S.A.* **104**, 16910–16915 (2007).
16. R. M. Blundred, G. S. Stewart, DNA double-strand break repair, immunodeficiency and the RIDDLE syndrome. *Expert Rev. Clin. Immunol.* **7**, 169–185 (2011).
17. S. Pinato *et al.*, RNF168, a new RING finger, MIU-containing protein that modifies chromatin by ubiquitination of histones H2A and H2AX. *BMC Mol. Biol.* **10**, 55 (2009).
18. R. Ceccaldi, B. Rondinelli, A. D. D'Andrea, Repair pathway choices and consequences at the double-strand break. *Trends Cell Biol.* **26**, 52–64 (2016).
19. Y. Fujioka *et al.*, Phase separation organizes the site of autophagosome formation. *Nature* **578**, 301–305 (2020).
20. L. D. Gallego *et al.*, Phase separation directs ubiquitination of gene-body nucleosomes. *Nature* **579**, 592–597 (2020).
21. Y.-L. Wang *et al.*, MRNIP condensates promote DNA double-strand break sensing and end resection. *Nat. Commun.* **13**, 2638 (2022).
22. C. Qin *et al.*, RAP80 phase separation at DNA double-strand break promotes BRCA1 recruitment. *Nucleic Acids Res.* **51**, 9733–9747 (2023).
23. M. Altmeyer *et al.*, Liquid demixing of intrinsically disordered proteins is seeded by poly(ADP-ribose). *Nat. Commun.* **6**, 8088 (2015).
24. Z. Liu *et al.*, Par complex cluster formation mediated by phase separation. *Nat. Commun.* **11**, 2266 (2020).
25. S. Kilic *et al.*, Phase separation of 53BP1 determines liquid-like behavior of DNA repair compartments. *EMBO J.* **38**, e101379 (2019).
26. L. Zhang *et al.*, 53BP1 regulates heterochromatin through liquid phase separation. *Nat. Commun.* **13**, 360 (2022).
27. F. Pessina *et al.*, Functional transcription promoters at DNA double-strand breaks mediate RNA-driven phase separation of damage-response factors. *Nat. Cell Biol.* **21**, 1286–1299 (2019).
28. Y. Shin *et al.*, Spatiotemporal control of intracellular phase transitions using light-activated optoDroplets. *Cell* **168**, 159–171.e14 (2017).
29. D. Sun, R. Wu, J. Zheng, P. Li, L. Yu, Polyubiquitin chain-induced p62 phase separation drives autophagic cargo segregation. *Cell Res.* **28**, 405–415 (2018).
30. S. Panier *et al.*, Tandem protein interaction modules organize the ubiquitin-dependent response to DNA double-strand breaks. *Mol. Cell* **47**, 383–395 (2012).
31. A. Patel *et al.*, A liquid-to-solid phase transition of the ALS protein FUS accelerated by disease mutation. *Cell* **162**, 1066–1077 (2015).
32. D. Bracha *et al.*, Mapping local and global liquid phase behavior in living cells using photo-oligomerizable seeds. *Cell* **175**, 1467–1480.e13 (2018).
33. C. Lukas, J. Falck, J. Bartkova, J. Bartek, J. Lukas, Distinct spatiotemporal dynamics of mammalian checkpoint regulators induced by DNA damage. *Nat. Cell Biol.* **5**, 255–260 (2003).
34. M. T. S. Mok, A. S. L. Cheng, B. R. Henderson, The ubiquitin ligases RNF8 and RNF168 display rapid but distinct dynamics at DNA repair foci in living cells. *Int. J. Biochem. Cell Biol.* **57**, 27–34 (2014).
35. S. F. Banani, H. O. Lee, A. A. Hyman, M. K. Rosen, Biomolecular condensates: Organizers of cellular biochemistry. *Nat. Rev. Mol. Cell Biol.* **18**, 285–298 (2017).
36. R. Oshidari *et al.*, DNA repair by Rad52 liquid droplets. *Nat. Commun.* **11**, 695 (2020).
37. L.-P. Bergeron-Sandoval, N. Safaee, S. W. Michnick, Mechanisms and consequences of macromolecular phase separation. *Cell* **165**, 1067–1079 (2016).
38. A. Jain, R. D. Vale, RNA phase transitions in repeat expansion disorders. *Nature* **546**, 243–247 (2017).
39. M. Du, Z. J. Chen, DNA-induced liquid phase condensation of cGAS activates innate immune signaling. *Science* **361**, 704–709 (2018).
40. S. Yasuda *et al.*, Stress- and ubiquitylation-dependent phase separation of the proteasome. *Nature* **578**, 296–300 (2020).
41. F. Pessina *et al.*, DNA damage triggers a new phase in neurodegeneration. *Trends Genet.* **37**, 337–354 (2021).
42. A. S. Singatulina *et al.*, PARP-1 activation directs FUS to DNA damage sites to form PARG-reversible compartments enriched in damaged DNA. *Cell Rep.* **27**, 1809–1821.e5 (2019).
43. C. Doil *et al.*, RNF168 binds and amplifies ubiquitin conjugates on damaged chromosomes to allow accumulation of repair proteins. *Cell* **136**, 435–446 (2009).
44. M. Wei, X. Huang, L. Liao, Y. Tian, X. Zheng, SENP1 decreases RNF168 phase separation to promote DNA damage repair and drug resistance in colon cancer. *Cancer Res.* **83**, 2908–2923 (2023).
45. J. Shi *et al.*, NOP53 undergoes liquid–liquid phase separation and promotes tumor radio-resistance. *Cell Death Discov.* **8**, 436 (2022).
46. A. Gaudreau-Lapierre *et al.*, Investigation of protein recruitment to DNA lesions using 405 nm laser micro-irradiation. *J. Vis. Exp.* **133**, 57410 (2018), 10.3791/57410.